Dalton Transactions

Accepted Manuscript

ROYAL SOCIETY OF CHEMISTRY

www.rsc.org/dalton

Vanadyl calix[6]arene complexes: Synthesis, structural studies and ethylene homo-(co-)polymerization capability

Carl Redshaw,[a*] Mark Walton,[b] Kenji Michiue,[c] Yimin Chao,[b] Alex Walton,[d] Pertti Elo,[e] Victor Sumerin,[e] Chengying Jiang[f] and Mark R.J. Elsegood[f]

[a] *Department of Chemistry, University of Hull, Hull, HU6 7RX, U.K.*

[b] *School of Chemistry, University of East Anglia, Norwich, NR4 7TJ, U.K.*

[c] *Process Technology Center*, *Mitsui Chemicals Inc., 580-32 Nagaura, Sodegaura, Chiba 299-0265, Japan*

[d] *School of Physics & Astronomy, University of Leeds, Leeds, LS2 9JT, UK.*

[e] *Borealis Polymers Oy, P.O. Box 330, Porvoo, FI-06101, Finland*

[f] *Chemistry Department, Loughborough University, Loughborough, Leicestershire, LE11 3TU, U.K.*

Abstract: Treatment of *p-tert*-butylcalix[6]areneH_6 (L^6H_6) with *in-situ* [LiVO(O*t*-Bu)$_4$] afforded, after work-up, the dark green complex [Li(MeCN)$_4$][V_2(O)$_2$Li(MeCN)(L^6H_2)$_2$]·8MeCN (**1**·8MeCN). On one occasion, the reaction led to the formation of a mixture of products, the bulk of which differing from **1** only in the amount of solvate, *viz* **2**·9.67MeCN. The second minor yellow product has the formula {[(VO_2)$_2$(L^6H_2)(Li(MeCN)$_2$)$_2$]·2MeCN}$_n$ (**3**·2MeCN), and comprises a 1D polymeric structure with links through the L^6H_2 ligand and Li_2O_2 units. When the reverse order of addition was employed such that lithium *tert*-butoxide (7.5 equivalents) was added to L^6H_6, and subsequently treated with $VOCl_3$ (2 equiv.), the complex {[VO(THF)][VO(μ-O)]$_2$Li(THF)(Et_2O)][L^6]}·2Et_2O·0.5THF (**4**·2Et_2O·0.5THF), which contains a trinuclear motif possessing a central octahedral vanadyl centre linked via oxo bridges to two tetrahedral (C_{3v}) vanadyl centres, was isolated. The calix[6]arene in **4** is

severely twisted and adopts a 'down, down, down, down, out, out' conformation. Use of excess lithium *tert*-butoxide led to a complex very similar to **4**, differing only in the solvent of crystallization, namely **5**·Et_2O·2THF. The ability of **1** and **5** to act as pre-catalysts for ethylene polymerization in the presence of a variety of co-catalysts and under various conditions has been investigated. Co-polymerization of ethylene with propylene and with 1-hexene have also been conducted; results are compared *versus* $VO(OEt)Cl_2$.

Keywords: Vanadyl; calix[6]arene; ethylene polymerization; ethylene/1-hexene co-polymerization; ethylene/propylene co-polymerization; homogenous; heterogeneous.

Introduction

In recent years, there has been considerable interest in the use of calix[*n*]arenes in a variety of catalytic/polymerization processes. [1] Indeed, it was Floriani some time ago who recognized that for the calix[4]arene ligand system, the four oxygen donors of the lower-rim, pre-organized in a quasi-planar geometry, offered an ideal opportunity for modelling oxo surfaces and thereby heterogeneous catalysts. [2] In the case of vanadium-based calixarene catalysis, Limberg *et al* have screened such systems for the oxidative dehydrogenation of short chain alkanes and alcohols, [3] whilst our group has screened a range of vanadyl-containing calix[*n*]arenes for α-olefin homo-(co-)polymerization. [4] Much of the work (about 80 %) in the literature has focused on the 'simplest' of the calixarene family, namely p-*tert*-butylcalix[4]areneH_4, due partly to its ease of preparation, and hence relatively low cost. Upon metallation, the calix[4]arene ligand set tends to bind to only one metal and retains a cone conformation. [5] The coordination chemistry associated with larger calix[*n*]arenes (n > 4) has been less well studied, particularly that of the calix[6]arene system. [6, 7] However, despite the often increased costs associated with the preparation of these larger ligands, their increased conformational

flexibility, presence of multiple cavities and ability to coordinate simultaneously multiple metal centres, means that such systems are proving to be of increased interest. In terms of catalysis, the ability to coordinate multiple metal centres in close proximity has the potential to lead to useful cooperative effects. [8] In recent papers on chromium(III) and iron(III) p-*tert*-butylcalix[4 and 6]arene chemistry, we have described the difficulties associated with the use of alkali metal alkoxides, and the resulting structural complications. [9, 10] Herein, similar use of lithium alkoxides also leads to some intriguing vanadium calix[6]arene structures (see scheme 1) ; structural reports of vanadium complexes of the larger calix[*n*]arenes remain scant. [3, 4] Vanadium-based systems α-olefin homo- and co-polymerizations continue to attract attention. [11] Screening for ethylene homo- and co-polymerization (with 1-hexene and with propylene) and the use of modified silica supported systems is discussed herein. Industrially, the co-polymerization of ethylene with higher olefins has been successfully achieved by employing group IV-based constrained geometry catalysts. [12] Dow Chemicals has also utilized complexes bearing imino-enamido or pyridyl-amido ligation for ethylene/1-olefin copolymerization and polyolefin block copolymer formation. [13]

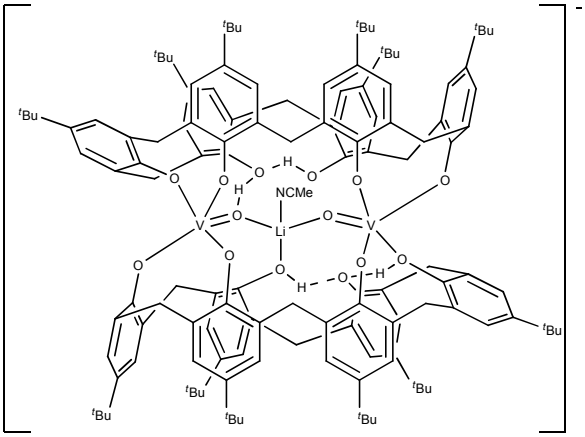

1.8MeCN; **2**.9.69MeCN

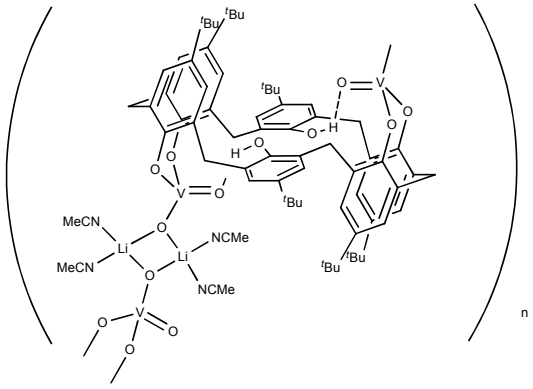

3.2MeCN

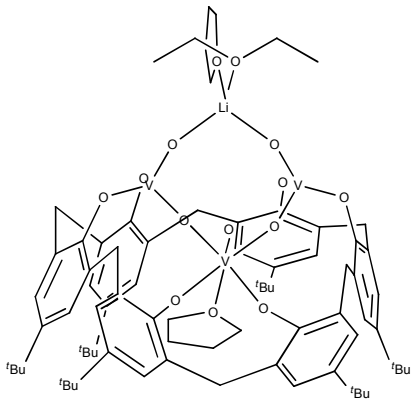

4·0.5(THF)·2Et_2O; **5**·2(THF)·Et_2O

Scheme 1. Vanadium calix[6]arene complexes prepared herein.

Results and Discussion

The heterobimetallic vanadium(V) / alkali metal reagent [LiVO(O*t*-Bu)$_4$], was synthesised by an adaptation of a procedure described by Wilkinson and co-workers, [14] whereby [$VOCl_3$] and four equivalents of LiO*t*-Bu were stirred in diethylether (or THF) at –78 ^oC for 12 h. Reaction of this vanadyl salt (two equivalents) with *p-tert*-butylcalix[6]areneH_6, L^6H_6, afforded, following work up with acetonitrile, dark green blocks of [Li(MeCN)$_4$][$V_2(O)_2$Li(MeCN)(L^6H_2)$_2$]·8MeCN (**1**·8MeCN) in good yield (*ca*. 60 - 65 %). Crystals of **1**·8MeCN suitable for single crystal X-ray diffraction studies

were grown from a saturated acetonitrile solution on prolonged standing (1 – 2 days) at ambient temperature. The molecular structure of complex **1** is presented in Figure 1, and selected bond lengths and angles are given in Table 1; crystallographic data are collated in Table 9.

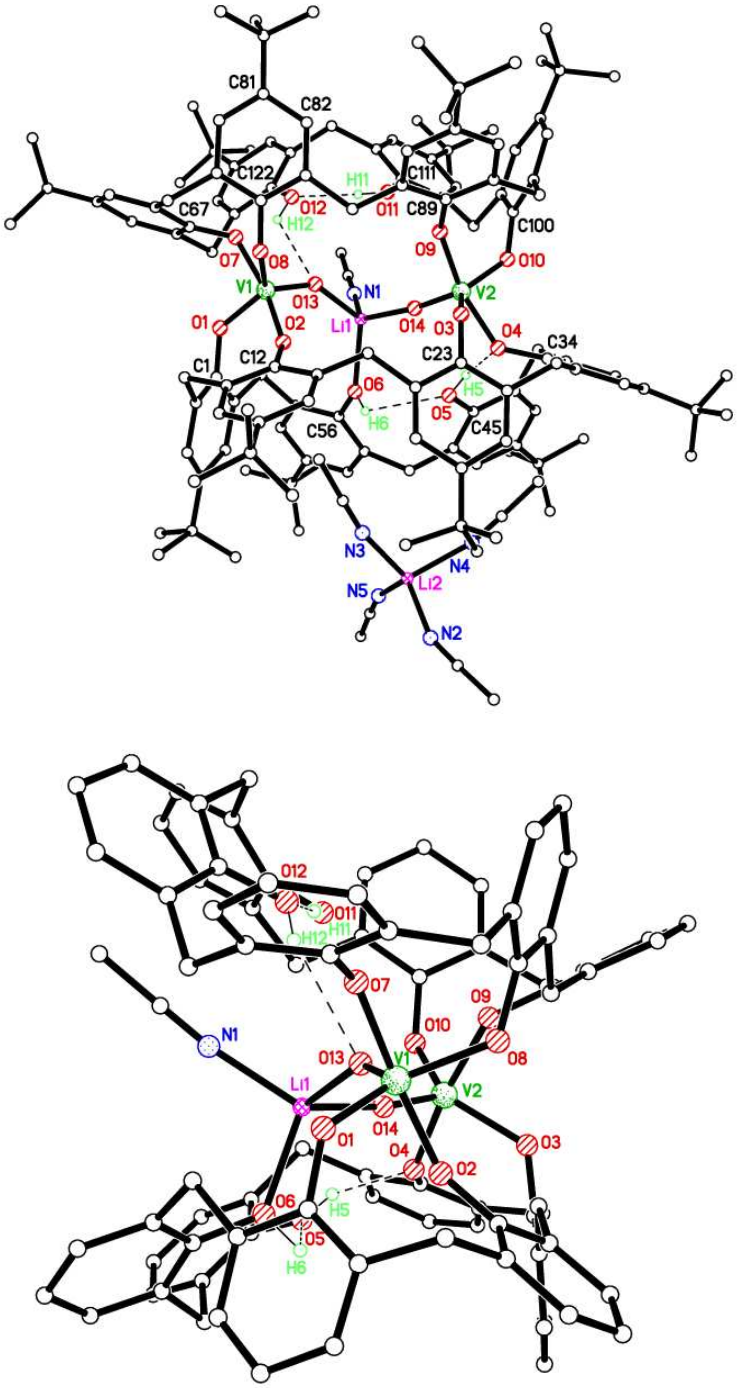

Figure 1. Above: structure of the salt $[Li(MeCN)_4][V_2(O)_2Li(MeCN)(L^6H_2)]\cdot 8MeCN$ (**1**·8MeCN) showing the atom numbering scheme. Hydrogen atoms except those involved in H-bonds, and non-coordinated solvent molecules have been omitted for clarity; below: structure of the anion with *tert*-butyl groups omitted for clarity, viewed approx. perpendicular to the top figure.

Table 1. Selected structural data for **1** and **2.**

Bond length (Å)/Angle (°)	**1**	**2**
V1-O1	1.861(4)	1.854(7)
V1-O2	1.805(5)	1.810(7)
V1-O13	1.606(4)	1.610(7)
V1-O7	1.916(4)	1.919(6)
V1-O8	1.870(4)	1.864(6)
Li1-O6	2.078(12)	2.07(2)
Li1-O13	1.948(11)	1.945(18)
O1-V1-O13	113.29(19)	112.4(3)
O2-V1-O7	168.17(18)	168.8(3)
V1-O1-C1	126.3(4)	127.1(6)
V1-O2-C12	144.9(4)	144.0(6)
V1-O7-C67	134.3(4)	133.5(6)
V1-O8-C78	125.6(4)	125.1(6)
V1-O13-Li1	143.1(4)	143.7(8)

Each L^6H_2 ligand coordinates via two pairs of adjacent oxygen atoms to two 5-coordinate vanadium centres, the remaining (per L^6) two oxygen atoms are still protonated and form O–H···O intramolecular hydrogen bonds. The geometry at each vanadium(V) centre is best described as a pseudo square-based pyramid with the bridging oxo atom (O13 for V1 and O14 for V2) at the apex. The Reedijk criteria confirmed this geometry assignment (τ = 0.64 for V1 and 0.55 for V2). [15] The two oxo groups are bridged by a 4-coordinate lithium cation, whose coordination sphere is completed

by an acetonitrile molecule and the protonated calixarene oxygen O6. A further lithium cation is required to balance the overall charge, and this lithium is found not to be bound to the anionic complex, but coordinated by only four acetonitrile ligands, and resides just inside one of the calixarene cavities.

A similar reaction on a separate occasion led, following work-up, to a mixture of green blocks as the major product (*ca.* 90 %) and a yellow minor product (*ca.* 10 %). The ^{1}H NMR data for the major green product was similar to that observed for **1**, and indeed the molecular structure namely $[Li(MeCN)_4][V_2(O)_2Li(MeCN)\ (L^6H_2)_2]\cdot 9.67MeCN$ (**2**·9.67MeCN) was found to be very similar, differing only in the degree of solvation. A view of the structure of **2** is shown in the ESI (Figure S1; selected bond lengths and angles are given in Table 1 and are compared with **1**. As for **1**, each vanadium centre adopts a pseudo square-based pyramid; Reedijk criteria confirmed this geometry assignment (τ = 0.64 for V1 and 0.55 for V2). [15] There is intramolecular H-bonding from phenol groups to neighboring phenol/phenolic oxygens, however the H atom H6 on the phenol bound to Li1 does not make an H-bond as there is no suitable acceptor nearby. The cation sits in one cavity of the L^6H_2 ligand, whilst the two acetonitrile molecules containing N14 and N15 sit in the other cavity; all remaining acetonitriles are *exo*.

The reaction flask also contained a small amount (*ca.* 10 %) of small yellow prisms. The molecular structure is shown in Figure 2 (selected bond lengths and angles are given in the caption; crystallographic data are collated in Table 9) revealed this minor product to be a 1D polymeric structure with links through the L^6H_2 ligand and diamond-shaped Li_2O_2 units, with the latter bridging the calixarene bound metal centres. The chains run parallel to the crystallographic *a* axis. The asymmetric unit contains half an L^6H_2 ligand, VO_2, $Li(MeCN)_2$ and a solvent (MeCN) of crystallization. The overall formula is $\{[(VO_2)_2(L^6H_2)(Li(MeCN)_2)_2]\cdot 2MeCN\}_n$ **3**·2MeCN, in which

each L^6H_2 ligand binds two pseudo tetrahedral vanadium centres. The L^6H_2 ligand adopts a chair conformation with two phenolates 'up', two 'down' and two 'flat'. The protonated phenolic groups of L^6H_2 are involved in H-bonding to the V=O groups across the calixarene cavity.

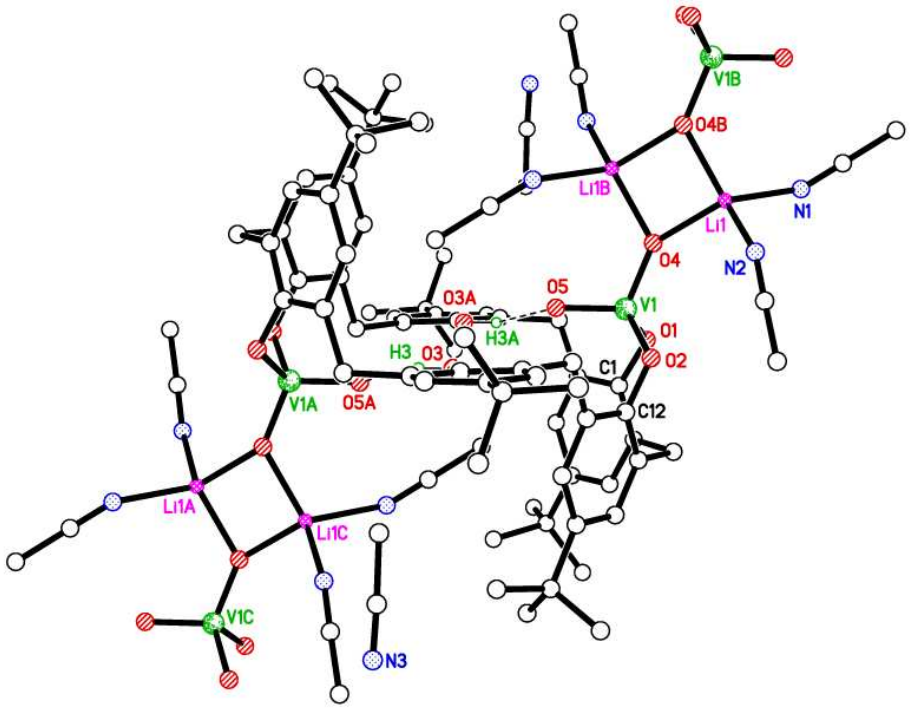

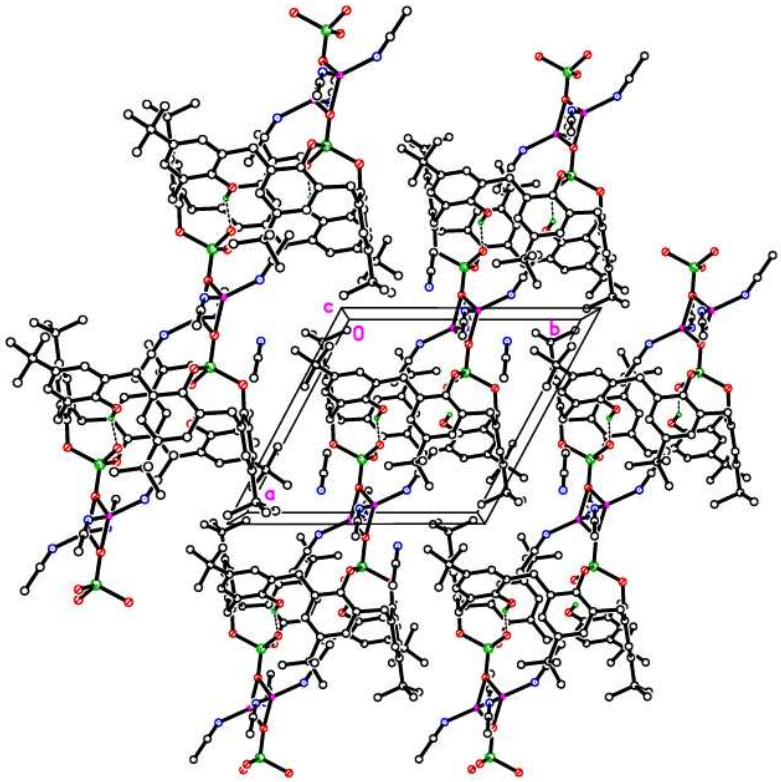

Figure 2. Above: structure of $\{[(VO_2)_2(L^6H_2)(Li(MeCN)_2)_2]\cdot 2MeCN\}_n$ (**3**·2MeCN), showing the atom numbering scheme. Hydrogen atoms except those involved in H-bonds have been omitted for clarity; below: chains of **3** running parallel to the crystallographic *a* axis. Selected bond lengths (Å) and angles (°): V(1) – O(1) 1.814(3), V(1) – O(2) 1.816(3), V(1) – O(4) 1.652(3), V(1) – O(5) 1.612(3), Li(1) – O(4) 1.973(8), Li(1B) – O(4) 1.972(8); O(4) – V(1) – O(5) 111.55(15), V(1) – O(1) – C(1) 120.3(2), V(1) – O(2) – C(12) 124.2(2), V(1) – O(4) – Li(1) 141.9(3), V(1) – O(4) – Li(1B) 1285(3).

When the reverse order of addition was employed such that lithium *tert*-butoxide (7.5 equivalents) was added to L^6H_6, and subsequently treated (at –78 °C) with two equivalents of $VOCl_3$, crystallization from tetrahydrofuran (THF) afforded the complex $\{[VO(THF)][VO(\mu\text{-}O)]_2Li(THF)(Et_2O)][L^6]\}\cdot 2Et_2O\cdot 0.5THF$ (**4**·2Et$_2$O·0.5THF). In **4**, the calix[6]arene adopts a 'down,

down, down, down, out, out' conformation (see Figure 3), which supports a trinuclear motif containing two tetrahedral vanadyl centres linked via an octahedral vanadyl centre. This trinuclear motif is reminiscent of that observed in the anionic part of the dioxo-imido complex $\{[(VN\textit{t}Bu)(THF)_{0.39}(O\textit{t}Bu)_{0.61}][(VO)(\mu\text{-}O)]_2L^6\}[\textit{t}BuNH_3]$, which was obtained on reaction of L^6H_6 with $[V(N\textit{t}Bu)(O\textit{t}Bu)_3]$. [4a] The geometrical parameters of **4** and this dioxoimido complex are compared in scheme 2 below, and reveal the similarities of the two trinuclear motifs.

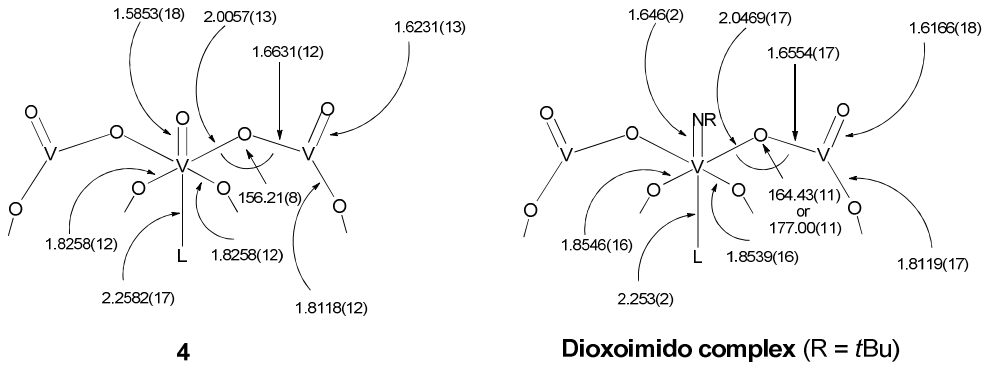

4 **Dioxoimido complex** (R = *t*Bu)

Scheme 2. Comparison of selected bond lengths of **4** *versus* the dioxoimido complex $\{[(VN\textit{t}Bu)(THF)_{0.39}(O\textit{t}Bu)_{0.61}][(VO)(\mu\text{-}O)]_2L^6\}[\textit{t}BuNH_3]$. [4a]

Molecules of **4** interlock in layers in the 1 0 1 plane (see ESI, Figure S2), whilst the solvent of crystallization are all positioned *exo* to the calixarene cages.

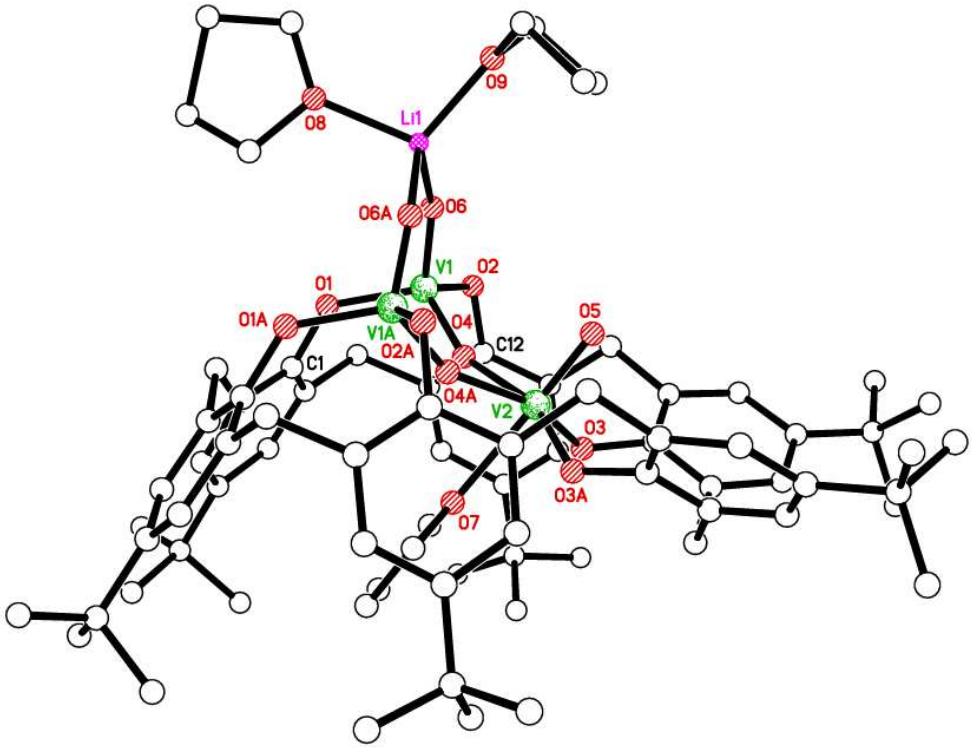

Figure 3. View of **4** revealing calix[6]arene 'down, down, down, down, out, out' conformation.

Increasing the amount of lithium *tert*-butoxide to 15 equivalents resulted in the isolation of a different solvate of **4**, namely $\{[VO(THF)][VO(\mu\text{-}O)]_2Li(THF)(Et_2O)][L^6]\}\cdot Et_2O$ (**5**·Et_2O·2THF). A view of the molecular structure of compound **5** is presented in Figure 4 (top), together with a picture of the core in Figure 4 (bottom); selected bond lengths and angles are given in Table 2 and are compared with those of complex **4**. It is evident that the geometrical parameters of both **4** and **5** are closely matched, and both molecules lie on mirror planes.

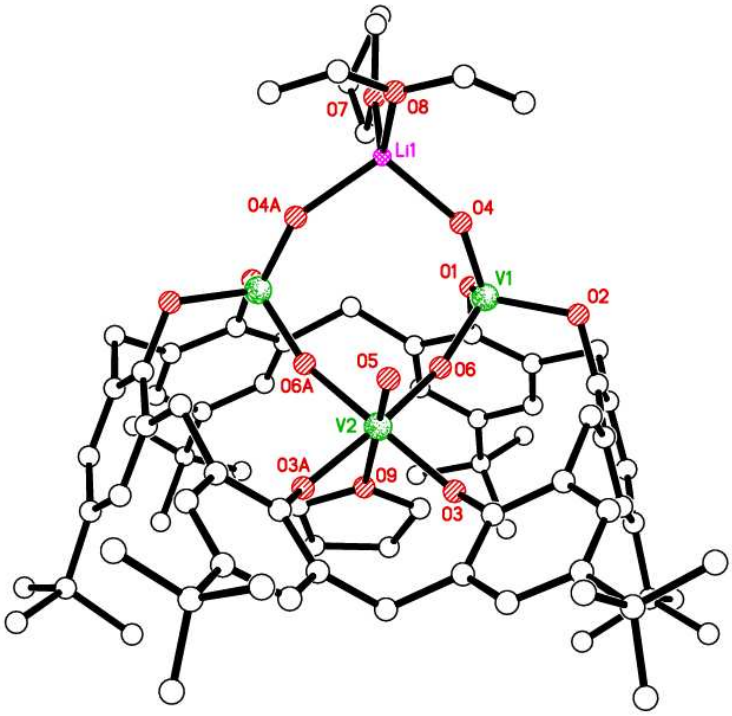

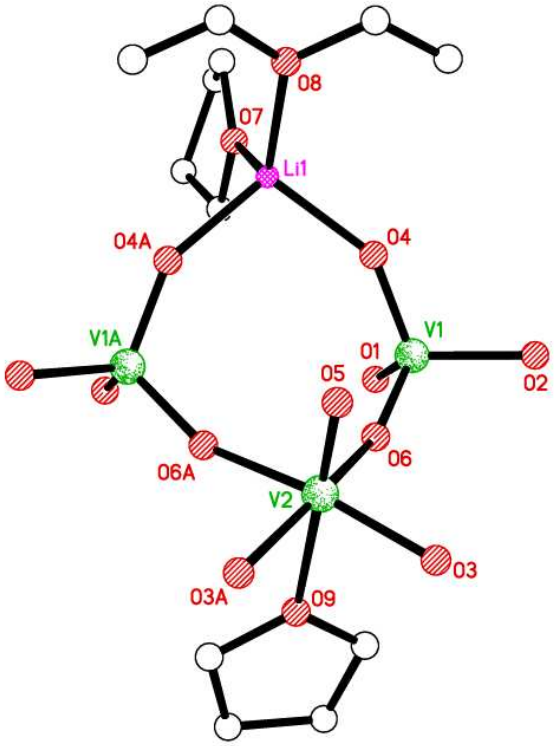

Figure 4. Above: structure of {[VO(THF)][VO(μ-O)]$_2$Li(THF)(Et$_2$O)][L^6]}·Et$_2$O (**5**·Et$_2$O·2THF), showing the atom numbering scheme. Hydrogen atoms and uncoordinated solvent molecules have been omitted for clarity; below: core of **5.**

Table 2. Selected structural data for complexes **4** and **5**.

Bond length (Å)/Angle (°)	**4**	**5**
V1 – O1	1.8118(12)	1.805(2)
V1 – O2	1.8158(13)	1.815(2)
V1 – O4	1.6625(12)	1.657(2)
V1 – O6	1.6231(13)	1.625(2)
V2 – O3	1.8258(12)	1.823(2)
V2 – O5	1.5853(18)	1.591(3)
V2 – O4	2.0057(13)	2.013(2)
V2 – O7	2.2582(17)	2.266(3)
Li1 – O6	1.948(3)	1.947(5)
O1-V1-O2	112.70(6)	112.57(10)
V1-O4-V2	156.21(8)	155.93(14)
V1-O6-Li1	148.03(14)	148.2(2)

Silica Immobilisation

Silica supported catalysts, specifically the Phillips catalyst, are responsible for almost half of the global production of high density polyethylene. Given this, much effort has been devoted to the elucidation of the *modus operandi* of such systems, and in particular the active site population at the surface. [16] Complex **1** was supported on pre-treated silica by refluxing in toluene for 12 h (affording complex **S1**); the SiO_2 had been heated to 350 °C under dynamic vacuum for 48 h. The colour of the complex was transferred to the silica during reaction, and any unreacted complex was removed by washing with toluene. To quantitatively ascertain the amount of silica bound vanadium, X-ray photoelectron spectroscopy (XPS) was employed.

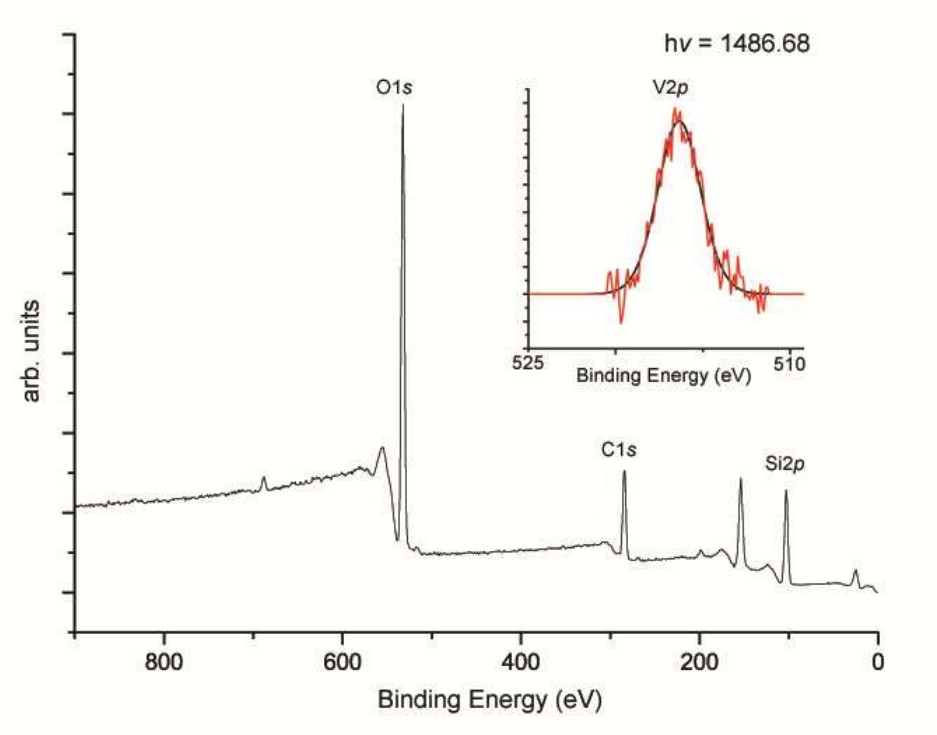

Figure 5 X-ray photoelectron survey spectrum of **S1**. The vanadium V2*p* energy window 525 – 510 eV is shown inset.

The XPS spectrum was calibrated to the C1*s* peak. Analysis of the photoelectron spectrum of **S1** (Figure 5) showed a single component at 516.3 ± 0.02 eV that was assigned to V2$p_{3/2}$. The XPS spectrum was consistent with the percentage of vanadium in the bulk sample at 0.24 %; the percentage of lithium in the sample could not be determined.

Catalytic screening

Ethylene

Preliminary Schlenk line screening: Complex **1** was found to be active for the polymerization of ethylene using methyl aluminium dichloride (MADC) as co-catalyst, in the presence of ethyltrichloroacetate (ETA) as re-activator. [13] The thermal stability of **1** peaked at *ca.* 60 ^{o}C. The use of dimethyl aluminium chloride (DMAC) as co-catalyst (Table 3, run 5) or lower equivalents of

MADC (Table 3, runs 1 - 2) was detrimental to the activity of the catalyst, as was the absence of ETA (Table 3, run 4).

Table 3 Ethylene polymerization results[a]

Run	Pre-catalyst[f]	Co-catalyst	Temp[g]	Yield[h]	Activity[i]
1[b]	**1** (0.25)	MADC	20	-	-
2[c]	**1** (0.25)	MADC	20	0.20	3.2
3	**1** (0.25)	MADC	20	0.78	12.5
4[d]	**1** (0.25)	MADC	20	0.24	3.8
5[e]	**1** (0.25)	DMAC	20	0.12	1.9
6	**1** (0.25)	MADC	60	0.86	13.8
7	**1** (0.25)	MADC	80	0.47	7.5

[a] Conditions: 1 bar ethylene, 15 min reaction time, co-catalyst MADC, 0.5mL ETA, Al/V (Molar ratio) 8000, [b] 2000 equivalents MADC, [c]4000 equivalents MADC, [d] No ETA added, [e] DMAC used as co-catalyst; [f](µmolV). [g] °C, [h] grams of polymer, [I] Kg/mmolV.h.bar.

*Screening of supported compound **S1***: The new supported compound S**1** was subjected to both polymerization (ethylene) and co-polymerization (ethylene and 1-hexene) using either triisobutyl aluminium (TIBA) or ethyl aluminium dichloride (EADC) as co-catalyst; ethyl trichloroacetate (ETA) was used as re-activator. Disappointingly the supported catalyst S**1** was found to be inactive for the polymerization of ethylene using either TIBA or EADC, both in the presence of the re-activator ETA, with monomer uptake resulting only from saturation of the solvent (Table S1, ESI).

The co-polymerization of ethylene and 1-hexene using **S1** was more successful. The activity of **S1** was found to peak at 3,050 g/mmol.h.bar using 80 °C and EADC as co-catalyst and in the presence of ETA (Table 4, run 2). Removal of ETA was detrimental to the activity as was the use of TIBA as co-catalyst (Table 4 and Table S2 in ESI). Re-runs of the catalytic screening showed a large spread of resultant activities, and a closer look at the consumption profile for **S1** showed the variance in activity could be the result of rapid de-activation of the metal centre.

The EDAC and ETA system had a much faster uptake of ethylene compared with the TIBA and EADC, however this uptake quickly subsided and the uptake of ethylene flat lined at ≈22 psi, indicating that the catalyst had been deactivated (Figure 6). A large variance in molecular weight was also found for each polymerization run.

Table 6 PPR - Ethylene/1-hexene Co-Polymerization Results with EADC and ETA[a]

Run	Pre-Catalyst (mg)	Metal Content[b]	Yield[c]	Activity[d]	Ethylene Uptake[e]	M_w[f]	T_m[g]	ETA: M ratio
1	**S1** (0.3)	0.014	0.068	2.42	54.9	173600	123.1	360
2	**S1** (0.3)[h]	0.014	0.086	3.05	71.1	262900	139.2	360
3	**S1** (0.3)	0.014	0.028	0.99	25.5	-	125.4	720
4	**S1** (0.3)[h]	0.014	0.047	1.68	40.8	218500	138.0	720
5	**S1** (0.3)	0.014	0.054	1.90	43.3	187300	138.9	1440
6	**S1** (0.3)[h]	0.014	0.040	1.41	33.7	-	137.9	1440
7	**S1** (0.3)[h]	0.014	0.017	0.60	16.3	-	-	1440
8	**S1** (0.3)[h]	0.014	0.016	0.56	16.2	-	-	1440
9	**S1** (0.8)	0.038	0.003	0.04	7.2	-	-	1440
10	**S1** (0.8)[h]	0.038	0.016	0.21	15.4	-	-	1440

[a] **Conditions**: 6.68 bar ethylene, 1 h reaction time, Al/V (Molar ratio) 4000; [b] µmol. [c] grams of polymer. [d] Kg/mmolV.h.bar [e] psi [f] weight average molecular weight, gmol^{-1}. [g] °C [h] repeated run

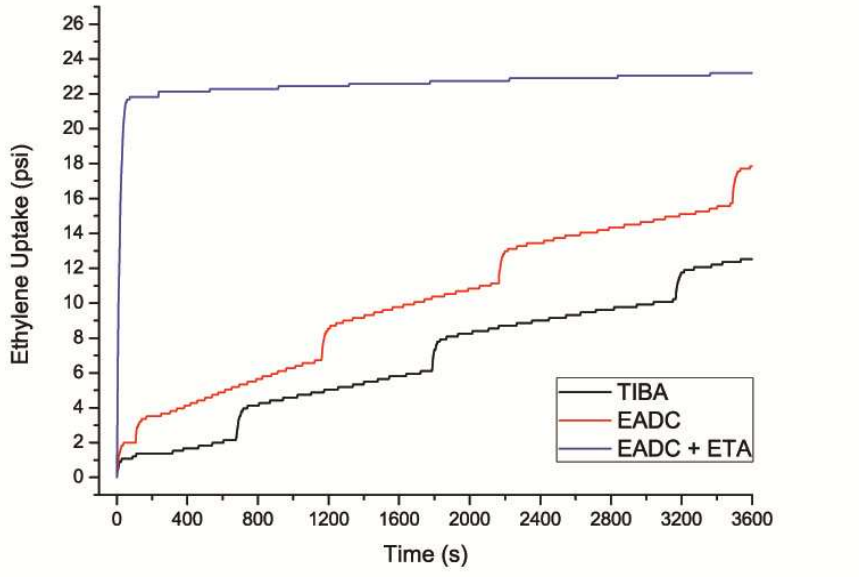

Figure 6. Consumption profiles for **S1**

Parallel Pressure Reactor Polymerization

Effect of temperature

Ethylene homopolymerization results are summarized in Table 7 and Figure 7; for ethylene uptake see Figures S3 and S4 in the ESI.

The activity using **1**/DMAC/ETA peaked at *ca* 80 ^{o}C (202.48 Kg/mmolV.h). This is distinctive character for **1**/DMAC/ETA, since the activity by other catalyst systems in this study dropped continuously on increasing the temperature from 50 ^{o}C to 140 ^{o}C (*vide infra*). As expected, the molecular weight (M_w) of the polyethylene rapidly dropped on increasing the temperature. Interestingly, the PDI values narrowed as the temperature increased, indicating that formation of thermodynamically favorable active species is promoted as the temperature is increased.

Similar use of DEAC as co-catalyst (see runs 5 - 8, Table 7) afforded lower activities than for DMAC, except for when operating at 140 ^{o}C (3.00 *versus* 1.16 Kg/mmolV.h). The number average molecular weight of the polyethylene obtained by **1**/DEAC/ETA are similar to those by **1**/DMAC/ETA, but the molecular weight distributions at 80 and 110 ^{o}C were much broader than those by DMAC, due to the formation of high molecular weight fractions (see ESI Figure S5 for GPC traces).

In the case of complex **5**, the observed catalytic activity in the presence of DMAC/ETA (runs 9 - 12, Table 7) was much lower than when using complex **1**. For **5**/DMAC/ETA, the notable thing is that ultrahigh molecular weight polyethylene was obtained at 50 ^{o}C (M_w: 1,544,400 g mol^{-1}) with the PDI value of 2.5, indicative of single-site catalysis. However the molecular weight (M_w) of the polyethylene dropped on increasing the temperature from 50 ^{o}C (1,544,400 g mol^{-1}) to 110 ^{o}C (49,100 g mol^{-1}). The use of DEAC as co-catalyst with the combination **5**/ETA led to even lower activities at temperatures ≤ 110 ^{o}C (see runs 13 - 16, Table 7).

Under the same conditions, the benchmark catalyst $VO(OEt)Cl_2$ with DMAC/ETA (runs 17 - 20, Table 7) afforded activities higher than those observed for **5**, but lower than those observed for **1**. At 140 ^oC, $VO(OEt)Cl_2$ was inactive under the conditions employed herein. In many of the runs, the polymer molecular weight (M_w) obtained using $VO(OEt)Cl_2$ was lower than that when employing either **1** or **5**. In the case of $VO(OEt)Cl_2$/DEAC/ETA (runs 21 - 24, Table 7), all activities were higher than when using **5**/DEAC/ETA, but were comparable with those observed when using **1**/DEAC/ETA. Interestingly, only the $VO(OEt)Cl_2$/DEAC/ETA system gave a high activity ratio (20 min/5min) of more than 1.0, indicating that this particular catalyst system has an induction period at 50 and 80 ^oC. The molecular weights (M_w) of the polymers obtained using either **1** or **5**/DEAC/ETA were far higher than those obtained when employing $VO(OEt)Cl_2$ at both 50 and 80 ^oC (M_w was not determined at either 110 or 140 ^oC for the $VO(OEt)Cl_2$ systems).

The above observations for the polymerization behavior indicate that the active species generated by **1**, **5** and $VO(OEt)Cl_2$ are different from each other.

^{13}C NMR spectral analysis of the polyethylene products indicated that there was no branching present (see ESI, Figure S6); the lower melting points ($\leq$ 130 ^oC) observed for some runs were thought to be due to the inclusion of lower molecular weights of the products obtained as opposed to the presence of branching.

Table 7. Ethylene polymerization results for complexes **1**, **5** and $VO(OEt)Cl_2$[a]

Run	Cat	Co-cat	Temp	Yield	Activity by weight[b]	Activity by C2 uptake (30 min)[b]	Activity by C2 uptake (5 min)[b]	M_w	M_n	PDI	
1	**1**	DMAC	50	0.306	122.36	50.21	107.59	640700	97700	6.6	134.2
2	**1**	DMAC	80	0.506	202.48	138.47	207.84	105200	40200	2.6	133.9
3	**1**	DMAC	110	0.171	68.48	37.88	178.89	30200	14400	2.1	133.9
4	**1**	DMAC	140	0.003	1.16	0.52	7.41	-	-	-	130.1
5	**1**	DEAC	50	0.256	102.24	50.72	69.55	489800	79000	6.2	130.7

6	**1**	DEAC	80	0.107	43.00	33.05	91.09	835300	40600	20.6	131.6
7	**1**	DEAC	110	0.039	15.60	9.82	47.33	198100	15300	13.0	133.2
8	**1**	DEAC	140	0.007	3.00	0.33	8.28	-	-	-	130.3
9	**5**	DMAC	50	0.132	52.65	30.25	41.45	1,544,400	609,400	2.5	135.6
10	**5**	DMAC	80	0.046	18.26	13.69	50.14	230,700	61,900	3.7	129.5
11	**5**	DMAC	110	0.010	4.16	2.01	20.22	49,100	13,800	3.6	132.4
12	**5**	DMAC	140	0.001	0.32	0.00	0.00				
13	**5**	DEAC	50	0.122	48.93	31.98	43.00	681,500	165,800	4.1	133.4
14	**5**	DEAC	80	0.007	2.64	1.00	10.78	294,700	30,400	9.7	129.5
15	**5**	DEAC	110	0.001	0.24	0.00	0.00				
16	**5**	DEAC	140	0.004	1.52	0.00	0.00				131.2
17	**Standard**	DMAC	50	0.374	74.72	39.44	56.86	945800	168700	5.6	134.7
18	**Standard**	DMAC	80	0.354	70.80	53.00	75.14	137600	45700	3.0	133.3
19	**Standard**	DMAC	110	0.097	19.36	15.50	71.87	-	-	-	134.5
20	**Standard**	DMAC	140	0.000	-	0.00	0.00	-	-	-	-
21	**Standard**	DEAC	50	0.483	96.70	69.13	34.47	316500	56800	5.6	134.4
22	**Standard**	DEAC	80	0.237	47.44	38.05	32.38	208700	27200	7.7	134.0
23	**Standard**	DEAC	110	0.087	17.34	12.83	44.27	-	-	-	133.8
24	**Standard**	DEAC	140	0.018	3.56	0.89	3.43	-	-	-	128.9

[a] **Conditions:** Runs conducted in toluene (5 ml) at over 30 min. All runs used 0.005 μmmol V, 0.8 MPa ethylene, 20,000 equivalents of ETA (v V) and 20,000 equivalents of co-catalyst (v V). Standard = $VO(OEt)Cl_2$. [b] Kg/mmolV.h.

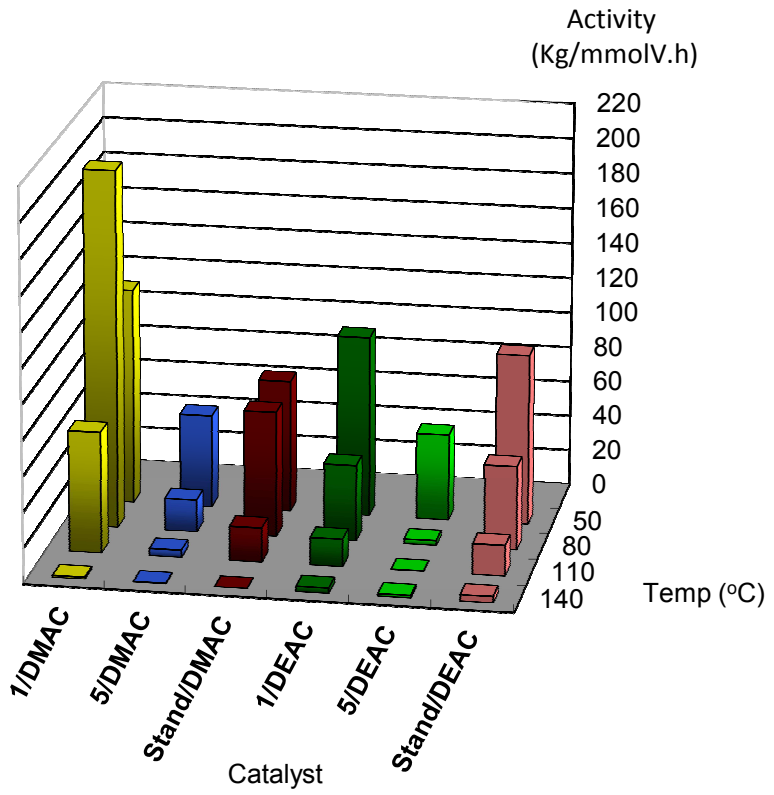

Figure 7. Activity in ethylene polymerization at 50 – 140 °C by **1**, **5** and the **Standard catalyst**.

Co-polymerization of ethylene with propylene (at 50 °C)

The co-polymerization of ethylene with propylene was conducted in the presence of DMAC or DEAC at 50 °C over 30 mins; results are presented in Table 8.

The system employing **1**/DMAC/ETA (run 1, Table 8) was found to possess far superior activity (107.08 Kg/mmolV.h) to that using **5**/DMAC/ETA (18.78 Kg/mmolV.h; run 4, Table 8), however both were found to be lower than the benchmark catalyst (156.24 Kg/mmlV.h; run 6, Table 8). The molecular weights (M_w) of the polymers obtained were 194,500 and 298,300 g mol^{-1} for **1** and **5**, respectively. The PDIs in each case were narrow (2.2 and 2.2), and the %C3 incorporation was 8.2 and 7.4 mol%, respectively.

Use of DEAC led to lower activities in both cases (**1** (run 2, Table 8) and **5** (run 5, Table 8)), although that for **1** (82.36 Kg/mmolV.h) was greater than that observed for the benchmark catalyst (76.36 Kg/mmolV.h; run 7, Table 8). Lower molecular weight (M_w) products were also obtained when DEAC was employed as an activator, though the PDIs were again narrow (*ca* 2.0), and the %C3 incorporation was 9.8 and 5.5 mol%, respectively (*versus* 9.1 for $VO(OEt)Cl_2$/DEAC/ETA (run 7, Table 8)).

In the case of **1**, use of Me_3Al (run 3, Table 8) as co-catalyst afforded an activity of 0.60 Kg/mmolV.h.

Table 8. Co-polymerization results of ethylene/propylene for complexes **1**, **5** and $VO(OEt)Cl_2$[a]

Run	Cat	Cat (μmol)	Co-cat	Yield	Activity by weight[b]	M_w	M_n	PDI	%C3[c]	T_m
1	**1**	0.005	DMAC	0.268	107.08	194500	90100	2.2	8.2	92.3
2	**1**	0.005	DEAC	0.206	82.36	63600	32300	2.0	9.8	89.8
3	**1**	0.005	Me_3Al	0.002	0.60	-	-	-	-	-
4	**5**	0.005	DMAC	0.047	18.78	298300	134500	2.2	7.4	92.5
5	**5**	0.005	DEAC	0.027	10.61	101200	50200	2.0	5.5	93.7
6	**Standard**	0.005	DMAC	0.391	156.24	241100	86600	2.8	10.0	88.9

7	**Standard**	0.005	DEAC	0.191	76.36	75700	42700	1.8	9.1	90.2

[a] **Conditions:** Runs conducted in toluene (5 ml) at 50 °C over 30 min. All runs used 0.005 μmmol V, 0.4 MPa ethylene, 0.4 MPa propylene, 20,000 equivalents of ETA (*v* V) and 20,000 equivalents of co-catalyst (*v* V). Standard = $VO(OEt)Cl_2$. [b] Kg/mmolV.h. [c] Mol% determined by IR.

Conclusion

In conclusion, use of the heterobimetallic complexes $[LiVO(O\textit{t}Bu)_4]$ with *p-tert*-butylcalix[6]arene led to the formation of highly crystalline vanadium complexes, which adopt new structural motifs, often stabilized by the presence of alkali metal cations. Such complexes will polymerize ethylene, in the presence of MADC and the re-activator ETA, with activities of the order of 10 Kg/mmol.h.bar. Activities fall off dramatically however, under heterogenous conditions (silica support), when using either TIBA or EADC as co-catalyst (and ETA), however better results were obtained for the co-polymerization of ethylene with 1-hexene (activity = 3.05 Kg/mmol.h.bar; however insufficient polymer was obtained to allow for FTIR measurements).

In a parallel pressure reactor, complexes **1** and **5** have been screened as pre-catalysts for the polymerization of ethylene in the presence of a variety of co-catalysts (with and without a re-activator) at various temperatures and for the co-polymerization of ethylene with propylene; results are compared *versus* the benchmark/standard pre-catalyst $VO(OEt)Cl_2$. In some cases, activities as high as 202.48 Kg/mmol.v.h were achievable, whilst is also proved possible to obtain higher molecular weight polymers (in comparable yields) *versus* the use $VO(OEt)Cl_2$. In the case of the co-polymerization, the incorporation of propylene was 5.5 – 9.8 mol% (*cf* 10 mol% for $VO(OEt)Cl_2$), though catalytic activities were lower. The ability of some of these vanadium calix[6]arenes to achieve high activity at high temperatures, whilst producing polymers with relatively high molecular weights (*cf* $VO(OEt)Cl_2$), makes them of possible industrial

interest. Further studies are now in progress to improve yet further the thermal stability of such calixarene-based systems with a view to their use in olefin polymerization catalysis.

Experimental

General:

All manipulations were carried out under an atmosphere of dry nitrogen using conventional Schlenk and cannula techniques or in a conventional nitrogen-filled glove box. Diethyl ether and tetrahydrofuran were refluxed over sodium and benzophenone. Toluene was refluxed over sodium. Dichloromethane and acetonitrile were refluxed over calcium hydride. All solvents were distilled and degassed prior to use. IR spectra (nujol mulls, KBr windows) were recorded on a Nicolet Avatar 360 FT IR spectrometer; ^{1}H NMR spectra were recorded at room temperature on a Varian VXR 400 S spectrometer at 400 MHz or a Gemini 300 NMR spectrometer or a Bruker Advance DPX-300 spectrometer at 300 MHz. The ^{1}H NMR spectra were calibrated against the residual protio impurity of the deuterated solvent. Elemental analyses were performed by the elemental analysis service at the London Metropolitan University. The ligands L^6H_6 was prepared as described in the literature. [18]

Synthesis of $[Li(MeCN)_4][V_2(O)_2Li(MeCN)(L^6H_2)_2]\cdot 8MeCN$ (**1**·8MeCN)

$[LiVO(O\textit{t}\text{-}Bu)_4]$ (prepared *in-situ* from $VOCl_3$ (0.27 mL, 2.89 mmol) and Li*O*t-Bu (0.93 g, 11.6 mmol), at –78 ^{o}C in 30 mL of THF) and L^6H_6 (1.40 g, 1.44 mmol) were dissolved in toluene (30 mL). The mixture was refluxed for 12 h. Following removal of solvent, the crude brown product was treated with acetonitrile (30 cm^3). Prolonged standing at room temperature afforded **1** as green blocks. Yield: 1.19 g, 63 %; elemental analysis calculated for **1**·3CH_3CN (sample dried *in-vacuo* for 12 h, leads to loss of 5MeCN), $C_{148}H_{184}Li_2N_8O_{14}V_2$: C 73.61, H 7.68, N 4.64 %; found: C 73.68, H 7.72, N 4.61 %;

IR (nujol mull, KBr): 3470bw, 2302w, 2272w, 2249w, 1747w, 1597m, 1416s, 1392s, 1362s, 1290s, 1261s, 1201s, 1152m, 1100bs, 1021bs, 977m, 949m, 915m, 871m, 835s, 799s, 771m, 760m, 728w, 695m, 680w, 635w, 617w cm^{-1}; MS (MALDI): *m/z* 2089 $[M]^+$ - 13MeCN, 2082 $[M]^+$ - 13MeCN - Li. ^1H NMR ($CDCl_3$) δ: 10.54 (2H, br s, O*H*), 7.37 (4H, d, 1.96 Hz, Ar-*H*), 7.26 (4H, d, 2.31 Hz, Ar-*H*), 7.16 (8H, m, Ar-*H*), 7.09 (4H, d, 2.31 Hz, Ar-*H*), 7.06 (4H, br s, Ar-*H*), 6.74 (2H, O*H*), 5.27 (4H, d, 13.9 Hz, *endo*-CH_2), 5.22 (2H, d, 20.3 Hz, *endo*-CH_2), 4.92 (4H, br s, *endo*-CH_2), 4.37 (2H, d, Ar-CH_2-Ar, 20.3 Hz, *endo*-CH_2), 4.31 (2H, d, 13.4 Hz, *exo*-CH_2), 3.50 (4H, d, 14.0 Hz, *exo*-CH_2), 3.45 (4H, d, 14.0 Hz, *exo*-CH_2), 3.07 (2H, d, 13.4 Hz, *exo*-CH_2), 1.28 (56H, overlapping s, *t*Bu-Ar). ^{51}V NMR ($CDCl_3$) δ: -70.5 ($\omega^1/_2$ 535 Hz, minor), –78.8 ($\omega^1/_2$ 770 Hz, major).

Data for $[Li(MeCN)_4][V_2(O)_2Li(MeCN)(L^6H_2)_2]\cdot 9.67MeCN$ (**2**·9.67MeCN) were as for **1** above.

$\{[(VO_2)_2(L^6H_2)(Li(NCMe)_2)_2]\cdot 2MeCN\}_n$ (**3**.2MeCN): Yield: *ca.* 10 %; elemental analysis calculated for **3**.1CH_3CN - CH_3CN, $C_{37}H_{46}LiN_2O_5V$: C 67.67, H 7.06, N 4.27 %; found: C 67.70, H 6.76, N 4.20 %; IR (nujol mull, KBr): 1603m, 1298m, 1285m, 1260s, 1235m, 1193s, 1108m, 1048m, 967m, 921m, 846m, 803m, 722m, 680w, 666w. MS (MALDI): *m/z* 1224 $[M]^+$ - 4MeCN - Li.

Synthesis of $\{[VO(THF)][VO(\mu\text{-}O)]_2Li(THF)(Et_2O)][L^6]\}\cdot 2Et_2O\cdot 0.5THF$ (**4**·2Et_2O·0.5THF)

To L^6H_6 (1.40 g, 1.44 mmol) in Et_2O (30 ml) at -78 °C was added LiO*t*-Bu (10.80 ml, 1.0 M in THF, 10.80 mmol), and the system was slowly allowed to warm to ambient temperature and left to stir for 12 h. The system was then cooled again to -78 °C, and then $VOCl_3$ (0.28 ml, 2.97 mmol) was added by syringe. The system was allowed to warm to ambient temperature and left to stir for 12 h. Filtration and cooling to -20 °C afforded **4** as orange tablets (on desolvation, the colour appears more grey-like).

Yield 0.74 g, 46.5 % (based on V). elemental analysis calculated for **4** (sample dried *in-vacuo* for 12 h, loss of 0.5THF + 2Et_2O), $C_{78}H_{104}LiO_{14}V_3$: C 65.72, H 7.35 %; found: C 63.61, H 7.70 % [19]; IR (nujol mull, KBr): 1603w, 1573w, 1483s, 1367s, 1301m, 1292m, 1259s, 1202m, 1156w, 1110m, 1092m, 1071m, 1020s, 976w, 946w, 913w, 871w, 803s, 770w, 722s, 689w, 670w. MS (ET, positive mode): *m/z* 1282 $[MH]^+$ - THF, 1208 $[MH]^+$ - THF – Li - VO. ^{1}H NMR (Acetoned_6) δ: 7.01 – 7.67 (8x m, 12H, Ar-*H*), 4.94 (d, $^2J_{HH}$ 12.0 Hz, 1H, *endo*-CH_2), 4.89 (d, $^2J_{HH}$ 12.0 Hz, 1H, *endo*-CH_2), 4.66 (d, 12.0 Hz, 1H, *endo*-CH_2), 4.44 (d, $^2J_{HH}$ 16.0 Hz, 1H, *endo*-CH_2), 4.42 (d, $^2J_{HH}$ 16.0 Hz, 1H, *endo*-CH_2), 4.32 (d, $^2J_{HH}$ 16.0 Hz, 1H, *endo*-CH_2), 3.58 (m, 8H, THF), 3.47 (d, $^2J_{HH}$ 12.0 Hz, 1H, exo-CH_2), 3.37 (d, $^2J_{HH}$ 12.0 Hz, 1H, *exo*-CH_2), 3.23 (d, $^2J_{HH}$ 12.0 Hz, 1H, *exo*-CH_2), 3.12 (d, $^2J_{HH}$ 16.0 Hz, 1H, *exo*-CH_2), 3.03 (d, $^2J_{HH}$ 16.0 Hz, 1H, *exo*-CH_2), 2.94 (d, $^2J_{HH}$ 16.0 Hz, 1H, *exo*-CH_2), 1.76 (m, 8H, THF), 1.29, 1.31, 1.25, 1.22, 1.15, 1.03 (6x s, 54H, *t*Bu-Ar).

Synthesis of {[VO(THF)][VO(μ-O)]$_2$Li(THF)(Et_2O)][L^6]}·Et_2O (**5**·Et_2O·2THF)

As for **4**, but using L^6H_6 (1.40 g, 1.44 mmol) and LiO*t*-Bu (21.60 ml, 1.0 M in THF, 21.60 mmol) affording **5** as a yellow solid in 27 % yield. Following drying *in-vacuo* (again the solid took on a grey-like appearance), characterization data for **5** were as for **4** above.

Polymer Characterization

The melt transition temperatures (T_m) of the polyethylene (PE) and ethylene/propylene copolymer (EPR) were determined by differential scanning calorimetry (DSC) with a Shimadzu DSC-60 instrument. The polymer samples were heated at 50 ^{o}C/min from 20 ^{o}C to 200 ^{o}C, held at 200 ^{o}C for 5 min, and cooled to 0 ^{o}C at 20 ^{o}C/min. The samples were held at this temperature for 5 min, and then reheated to 200 ^{o}C at 10 ^{o}C/min. The reported T_m was determined from the second heating scan unless otherwise noted. Molecular weights (M_w and M_n) and polymer disparity index (PDI) of PE and EPR

were determined using a Waters GPC2000 gel permeation chromatograph equipped with four TSKgel columns (two sets of TSKgelGMH$_6$-HT and two sets of TSKgelGMH$_6$-HTL) at 140 ^{o}C using polyethylene calibration. *o*-Dichlorobenzene (ODCB) was used as the solvent.

The propylene content of the EPR was measured by IR analysis using a JASCO FT-IR. [20]

Polymerization Procedure (Tables 3 and 4; and Tables S1 and S2)

A pre-weighed glass vial with stirring paddles was sealed and purged with ethylene. 5 μmol of co-catalyst from a 100 mM heptane solution was added along with co-monomer (if required). Heptane was then added to reach a volume of 4000 μL in the reaction vessel and heated to 80 °C. The ethylene pressure was set to 92 psi (6.34 bar) and the catalyst (along with ETA) was added as a heptane slurry. The run was left stirring for 60 minutes and quenched with CO_2 (35 % in N_2). The glass vial was dried by vacuum centrifuge and weighed.

Typical Parallel Pressure Reactor Polymerization Run (Tables 7 and 8)

Polymerization reactions were performed in a parallel pressure reactor (Argonaut Endeavor® Catalyst Screening System) containing 8 reaction vessels (15 mL) each equipped with a mechanical stirrer and monomer feed lines. At first, a toluene solution (and a toluene solution of ETA as necessary) was injected into each vessel. *For ethylene polymerization*, the solution was heated to the polymerization temperature (T_p) and thermally equilibrated, and the nitrogen atmosphere was replaced with ethylene and the solution was saturated with ethylene at the polymerization pressure. *For ethylene/propylene copolymerization*,-the nitrogen atmosphere was replaced with propylene and the reaction vessels were pressurized with propylene (0.4 MPa at 25 ^{o}C), and the solution was heated to the T_p and thermally equilibrated, then ethylene was introduced into the reactor up to the polymerization pressure. *In all*

cases the polymerization was started by addition of a toluene solution of alkyl aluminum or alkyl aluminum chloride followed by addition of a toluene solution of the vanadium complex (0.50 mL toluene solution of complex followed by 0.25 mL toluene wash). The total volume of the reaction mixture was 5 mL for all polymerizations. The pressure was kept constant by feeding ethylene on demand. After the reaction, the polymerization was stopped by addition of excess isobutyl alcohol. The resulting mixture was added to acidified methanol (45 ml containing 0.5 ml of concentrated HCl). The polymer was recovered by filtration, washed with methanol (2 × 10 ml) and dried in a vacuum oven at 80 ^{o}C for 10 h.

Crystallography.

This set of structures was particularly challenging, so we describe here the details of how the various problems were approached. Crystal data were collected on a Bruker SMART 1000 CCD diffractometer for **1**·8MeCN or a Bruker APEX 2 CCD diffractometer for **4**·2Et_2O·0.5THF and **5**·2(THF)·Et_2O using narrow slice 0.3° ω-scans [21]. Crystal data for **2**·9.67(C_2H_3N) and **3**·2C_2H_3N were collected using a rotating anode source on a Rigaku AFC12/Saturn724+ CCD diffractometer [22]. Data were corrected for Lp effects and for absorption, based on repeated and symmetry equivalent reflections [21], and solved by direct methods [23, 24]. Structures were refined by full matrix least squares on F^2 [23, 24]. H atoms were included in a riding model except for H(6) in **1**·8MeCN, H(9) in **2**·9.67(C_2H_3N) and H(3) in **3**·2C_2H_3N for which coordinates were freely refined. Hydrogen atom U_{iso} values were constrained to be 120 % of that of the carrier atom except for methyl and hydroxyl-H (150 %). All three structures exhibited either two-fold disorder in some *tert*-butyl groups and/or solvent molecules where restraints were applied to geometry and anisotropic displacement parameters. Some solvent molecules were diffuse and refined at fractional or half weight, so numbers of solvent molecules of crystallisation

should be regarded as approximate. Twinning is suspected in structures **1**·8MeCN and **3**·2MeCN, but no satisfactory twin model could be developed. The Platon Squeeze procedure was used to model badly disordered solvent molecules in **4**·2Et_2O·0.5THF (approx.one molecule of Et_2O and half a molecule of THF were 'squeezed') and in **5**·2(THF)·Et_2O (one THF was 'squeezed'). [24, 25] Further details are provided in Table 9. CCDC 895364 and 950038 – 950039 contain the supplementary crystallographic data for this paper. These data can be obtained free of charge from The Cambridge Crystallographic Data Centre via www.ccdc.cam.ac.uk/data_request/cif.

Acknowledgements

The EPSRC Mass Spectrometry Service (Swansea, UK) is thanked for data collection, and the EPSRC National X-ray Crystallography Service (Southampton) is thanked for data collection on **2**·9.69(MeCN) and **3**·2MeCN. CR also thanks the EPSRC for an overseas travel grant (EP/L012804/1).

Supporting Information Available: X-ray crystallographic files CIF format for the structure determinations of compound **1 – 5**.

Table 9. Crystallographic data for complexes **1**·8MeCN, **2**·9.67MeCN, **3**·2MeCN, **4**·0.5(THF)·2Et_2O and **5**·2(THF)·Et_2O.

Compound	**1**·8(CH_3CN)	**2**·9.67MeCN	**3**·2(CH_3CN)	**4**·0.5(THF)·2Et_2O	**5**·2(THF)·Et_2O
Formula	$C_{142}H_{175}Li_2N_5O_{14}V_2 \cdot 8CH_3CN$	$C_{142}H_{175}Li_2N_5O_{14}V_2 \cdot 9.67CH_3CN$	$C_{37}H_{46}LiN_2O_5V \cdot CH_3CN$	$C_{78}H_{104}LiO_{14}V_3 \cdot 0.5THF \cdot 2Et_2O$	$C_{78}H_{104}LiO_{14}V_3 \cdot 2THF \cdot Et_2O$
Formula weight	2620.06	2688.70	697.69	1609.66	1643.69
Crystal system	monoclinic	monoclinic	Triclinic	monoclinic	monoclinic
Space group	*C*2/*c*	*C*2/*c*	*P*$\bar{1}$	*I*2/*m*	*I*2/*m*
Unit cell dimensions					
a (Å)	61.082(3)	61.03(4)	12.0813(7)	18.1085(15)	30.746(14)
b (Å)	20.4495(10)	20.308(18)	12.7544(8)	16.6772(14)	16.851(6)
c (Å)	25.7085(12)	25.59(2)	14.2206	30.818(3)	18.040(7)
α (°)	90	90	90.879(6)	90	90
β (°)	90.0954(8)	90.11(2)	94.563(7)	97.4530(12)	96.972(6)
γ (°)	90	90	117.961(8)	90	90
V (Å^3)	32112(3)	31716(43)	1925.9(2)	9228.4(14)	9277(6)
Z	8	8	2	4	4
Temperature (K)	150(2)	100	100	150	150
Wavelength (Å)	0.71073	0.71073	0.71073	0.71073	0.71073
Calculated density (g.cm^{-3})	1.084	1.126	1.203	1.159	1.177
Absorption coefficient (mm^{-1})	0.176	0.180	0.301	0.357	0.357
Transmission factors (min./max.)	0.914 and 0.943	0.982 and 0.995	0.973 and 0.997	0.733 and 0.904	0.965 and 0.771
Crystal size (mm^3)	0.52 × 0.45 × 0.34	0.10 × 0.06 × 0.03	0.09 × 0.04 × 0.01	0.93 x 0.47 x 0.29	0.77 x 0.32 x 0.10
θ(max) (°)	25.0	22.5	25.0	30.6	26.6
Reflections measured	115060	132839	20767	54183	41592
Unique reflections	28282	20718	6765	14441	9949
R_{int}	0.0691	0.225	0.094	0.031	0.077
Reflections with $F^2 > 2\sigma(F^2)$	17140	14644	4354	10301	6347

Number of parameters	1883	1997	458	537	550
R_1 [$F^2 > 2\sigma(F^2)$]	0.1179	0.1724	0.0737	0.0481	0.0631
wR_2 (all data)	0.3571	0.3445	0.2118	0.1552	0.2050
GOOF, S	1.110	1.274	1.021	1.041	1.030
Largest difference peak and hole (e Å^{-3})	1.184 and –0.393	0.724 and -0.445	0.823 and -0.437	0.893 and -0.593	0.795 and -0.615

References

1. D. M. Homden and C. Redshaw, *Chem. Rev.*, **2008**, *108*, 5086.

2. L. Giannini, A. Caselli, E. Solari, C. Floriani, A. Chiesi-Villa, C. Rizzoli, N. Re, A. Sgamellotti, *J. Am. Chem. Soc*. **1997**, *119*, 9198.

3. (a) E. Hoppe, C. Limberg and B. Ziemer, *Inorg. Chem*., **2006**, *45*, 8308. (b) E. Hoppe, C. Limberg, B. Ziemer and C. Mügge, *J. Mol. Cat A: Chem*., **2006**, *251*, 34. (c) C. Limberg, *Eur. J. Inorg. Chem.* **2007**, 3303.

4. (a) V.C. Gibson, C. Redshaw and M.R.J. Elsegood, *J. Chem. Soc., Dalton Trans*., **2001**, 767. (b) C. Redshaw, M. A. Rowan, L. Warford, D. M. Homden, A. Arbaoui, M. R. J. Elsegood, S. H. Dale, T. Yamato, C. P. Casas and S. Matsui, *Chem. Eur. J.*, **2007**, *13*, 1090.

5. We note that it is also possible for the calix[4]arene ligand set to bind to more than one metal simultaneously, for a recent example see A. Crochet and K. M. Fromm, *Polyhedron* **2013**, 52, 610.

6. For pre-2002 calix[*n*]arenes coordination chemistry, see C. Redshaw, *Coord. Chem. Rev*., **2003**, *244*, 45; for post-2002 calix[*n*]arenes coordination chemistry, see (a) Y. Li, K-Q. Zhao, C. Redshaw, B.A. Martínez Ortega, A.Y. Nuñez and T.A. Hanna in *The Chemistry of Metal Phenolates*, Ed. J. Zabicky, Wiley, **2014**. ISBN 978-0-470-97358-5; (b) D.J. Hernández and I. Castillo, *Current Trends in X-ray Crystallography*, Ed. A. Chandrasekaran, InTech, **2011**. ISBN 978-953-307-754-3.

7. For recent examples of calix[8]arene coordination chemistry, see R.D. McIntosh, S.M. Taylor, S. Sanz, C.M. Beavers, S.J. Teat, E.K. Brechin and S.J. Dalgarno, *Dalton Trans*. **2011**, *40*, 12265 and references therein.

8. a) S. Singh and H. W. Roesky, *Dalton Trans.*, **2007**, 1360. b) M. P. Weberski, Jr, C. Chen, M. Delferro, and T. J. Marks, *Chem. Eur. J.* **2012***, 18*, 10715. c) M. Delferro, and T. J. Marks, *Chem. Rev.* **2011**, *111*, 2450–2485.

9. C. Redshaw, D. Homden, D. L. Hughes, J. A. Wright and M. R. J. Elsegood, *Dalton Trans*. **2009**, 1231-1242.

10. A. Arbaoui, C. Redshaw, M. R.J. Elsegood, V. E. Wright, A. Yoshizawa and T. Yamato, *Chem. Asian J*. **2010** *5*, 621.

11. See for example (a) Y. Onishi, S. Katao, M. Fujiki and K. Nomura, *Organometallics*, **2008**, *27*, 2590. (b) J. Q. Wu, L. Pan, N. H. Hu and Y. S. Li, *Organometallics*, **2008**, ***27***, 3840. (c) C. Redshaw, *Dalton Trans*., **2010**, *39*, 5595 and references therein. (d) D. Wang, Z. Zhao, T.B. Mikenas, X. Lang, L.G. Echevskaya, C. Zhao, M.A.Matsko and W. Wu, *Polym. Chem*, **2012**, *3*, 2377.

12. R.E. LaPointe, J.C. Stevens, P.N. Nickias and M.H. McAdon, Dow Chemicals USA, EP 0 520 732 B1, 1992.

13. (a) R. Figueroa, R.D. Froese, Y. He, J. Klosin, C.N. Theriault and K.A. Abboud, *Organometallics* **2011**, *30*,1695. (b) P.P.Fontaine, R. Figueroa,S.D.McCann, D.Mort and J. Klosin, *Organometallics* **2013**, *32*, 2963. (c) T.R. Boussie, G.M. Diamond, C. Goh, K.A. Hall, A.M. LaPointe, M.K. Leclerc, V. Murphy, J.A.W. Shoemaker, H. Turner, R.K. Rosen, J.C. Stevens, F. Alfano, V. Busico, R. Cipullo and G. Talarico, *Angew. Chem. Int. Ed*. **2006**, *45*, 3278. (d) P.S. Chum and K.W. Swogger, *Prog. Polym. Sci*., **2008**, *33*, 797. (e) For a recent review on the use of Post-Metallocenes catalysts for industrial polyolefin production, see M. C. Baier, M. A. Zuideveld and S.Mecking, *Angew. Chem. Int. Ed*. **2014**, *53*, 9722.

14. M. Bochmann, G. Wilkinson, G. B. Young, M. B. Hursthouse, K. M. A. Malik, *J. Chem. Soc., Dalton Trans.* **1980**, 1863.

15. A. W. Addison, T. N. Rao, J. Reedijk, J. Van Rijn, G. C. Verschoor, *J. Chem. Soc. Dalton Trans*. **1984**, 1349.

16. M.P. McDaniel, *Adv.in Cat*., **2010**, *53*, 123

17. The use of ETA is now well established, for early examples, see (a) A. Gumboldt, J. Helberg and G. Schleitzer, *Makromol. Chem.* **1967**, *101*, 229. (b) D.L. Christman, *J. Polym. Sci., Part A*, **1972**, *10*, 471. (c) E. Addison, A. Deffieux, M. Fontanille and K. Bujadoux, *J. Polym. Sci., Part A*, **1994**, *32*, 1033.

18. A. Arduini, A. Casnati in Macrocycle Synthesis (Ed.: D. Parker), Oxford University Press, **1996**, chap. 7.

19. Despite repeated analyses for **4** and **5**, there was no fit between the experimental and the calculated values. Microanalysis of calixarenes is problematic, see S. Camiolo, P.A. Gale, M.I. Ogden, B.W. Skelton and A.H. White, *J. Chem. Soc., Perkin Trans 2*, **2001**, 1294 and references therein.

20. C. Tosi and T. Simonazzi, *Angew. Macromol. Chem*. **1973**, *32*, 153.

21. SMART and SAINT software for CCD diffractometers. Bruker AXS Inc., Madison, USA, **2001**.

22. Rigaku CrystalClear-SM Expert 3.1 b10 software for CCD diffractometers. Rigaku, **2012**.

23. G.M. Sheldrick, SHELXTL user manual, version 6.10. Bruker AXS Inc., Madison, WI, USA, **2000**.

24. G.M. Sheldrick, *Acta Crystallogr*. **2008**, *A64*, 112.

25. A.L. Spek, *Acta Crystallogr*. **1990**, *A46*, C34.